RSC Advances

ROYAL SOCIETY OF CHEMISTRY

www.rsc.org/advances

Graphical Abstract

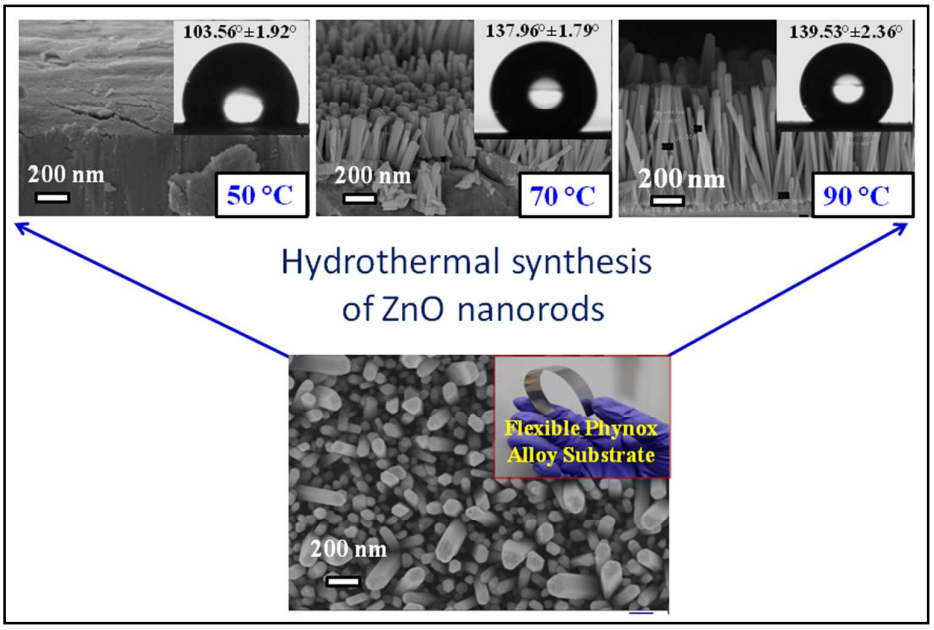

Synthesis of ZnO nanorods on flexible Phynox alloy substrate: Influence of growth temperature on their properties

Venkateswarlu Gaddam[a], R. Rakesh Kumar[a,b], Mitesh Parmar[a], M.M.Nayak[c] and K.Rajanna[*a]

[a] Department of Instrumentation and Applied Physics, Indian Institute of Science, Bangalore 560012, India.

[b] Department of Engineering Physics, Gitam Univeristy Hyderabad campus, Hyderbad-502329.

[c] Centre for Nanoscience and Engineering, Indian Institute of Science, Bangalore 560012, India.

Abstract

A novel flexible alloy substrate (Phynox, 50 μm thick) is used for the synthesis of Zinc Oxide (ZnO) nanorods by low-temperature solution growth method. The growth of ZnO nanorods were observed at low temperature range of 60-90 °C for the growth duration of 4 hours. As-synthesized nanorods were characterized by field-emission scanning electron microscopy (FE-SEM), X-ray diffraction (XRD), transmission electron microscopy (TEM), and X-ray photoelectron spectroscopy (XPS) for their morphology, crystallanity, microstructure and composition. The as-grown ZnO nanorods were observed to be relatively vertical to the substrate. However, the morphology of ZnO nanorods in terms of their length, diameter and aspect ratio is found to vary with the growth temperatures. The morphological variations are mainly due to the effects of varied relative growth rates with growth temperature. The growth temperature influenced ZnO nanorods are also used for analyzing their wetting (either hydrophobic or hydrophilic) property. After carrying out multiple wetting behaviour analysis, it has been found that the as-synthesized ZnO nanorods are hydrophobic in nature. These ZnO nanorods have the potential application possibilities in self cleaning devices, sensors & actuators as well as energy harvesters like nanogenerators.

Key words: Flexible phynox alloy substrate, ZnO nanorods, Low-temperature solution growth method, Temperature-controlled aspect ratios, Hydrophobicity.

*** Corresponding author**

E-mail: kraj@isu.iisc.ernet.in

Tel: +91-80-2293 3188, Fax: +91-80-2360 0135

Graphical Abstract

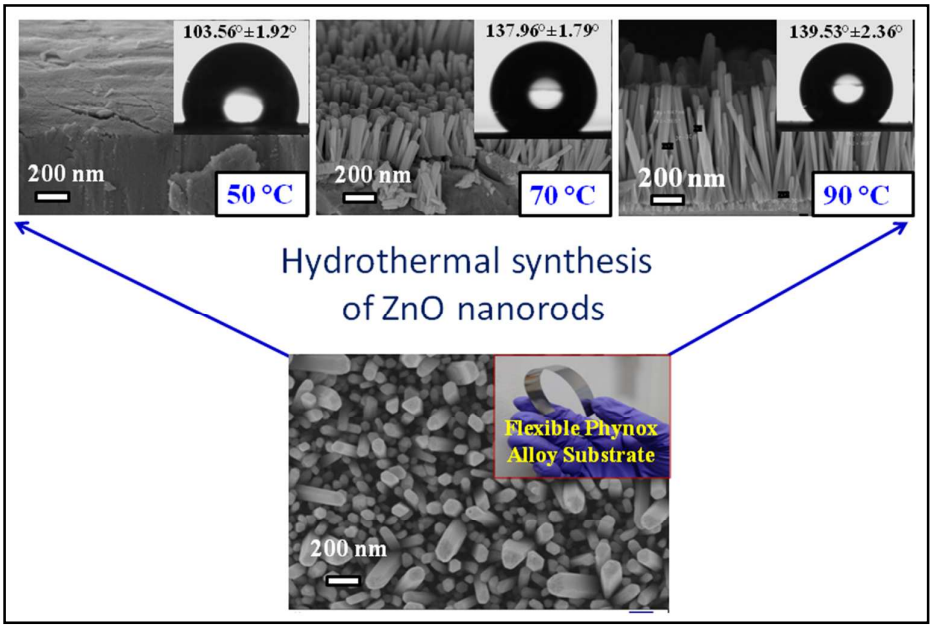

1. Introduction

Zinc Oxide (ZnO) is one of the most promising potential materials due to its remarkable properties such as wide band-gap (3.37eV), large exciton binding energy (60 meV), excellent chemical & thermal stability, transparency and biocompatibility. Due to the possible utilization of the above mentioned properties in various fields like electronics, optoelectronics, electrochemical and electromechanical, the ZnO has become more popular and drawing increasing interest in the area of nanotechnology [1-4]. ZnO is very flexible functional material exhibiting wide structural morphologies, such as nanocombs [5], nanorings [6], nanohelixes/nanosprings [7], nanobelts [8], nanowires/nanorods [9, 10], nanotubes [11], nanocages [12] and nanosheets [13]. Among these, one dimensional (1D) ZnO nanorords/nanowires have been extensively studied in the recent past due to their multifunctional device applications in the areas of ultraviolet (UV) lasers [14-15], light emitting diodes [16], field emission devices [17-18], solar cells [19-20], surface acoustic wave devices [21], piezoelectric sensors & actuators [22-23] and nanogenerators [2-3,24]. The 1D ZnO nanorods can be synthesized by various methods such as physical vapour deposition (PVD) [8], chemical vapour deposition (CVD) [25], metalorganic chemical vapour deposition (MOCVD) [26], molecular beam epitaxy (MBE) [27], pulsed laser deposition (PLD) [28], hydrothermal synthesis [3,24,29] and electrochemical deposition [30]. Among all these methods, solution growth assisted hydrothermal synthesis is most favourable due to its flexibility to carry out the synthesis process on variety of substrates (both conducting and non-conducting) at low temperatures (<100°C). Moreover, this process is relatively simple, cost effective, less hazardous and also most suitable for the uniform ZnO nanorods synthesis over larger surface area [3, 13, 29].

In any synthesis process, the choice of the substrate plays an important role in controlling the structure, orientation and density of the nanorods which directly affects their properties as well as their utility in the corresponding applications [31]. Hence, large-scale, low-cost and highly oriented 1D ZnO nanorods on various conducting flexible substrates is still expected for novel device applications [32]. Well-oriented vertically grown ZnO nanorods on metallic substrates are preferable for some of the device fabrications considering their improved electrical and thermal conduction. In addition to this, the electrically conductive substrate could act as one of the electrodes and hence reduce the fabrication complexities [33]. Moreover, sometimes the working mechanism and the device performance are also affected by the flexibility of the substrate itself. In recent years, most of the papers have reported on the synthesis of piezoelectric ZnO nanorods on various non-flexible substrate materials like Si, sapphire and ITO glass for nanogenerators. However, these non-flexible substrates suffer from the problem of very low electrical output response (piezoelectricity). Additionally, few investigations also carried out the study on piezoelectric ZnO nanostructures grown on polymer flexible substrates such as Polyethylene terephthalate (PET), Kapton, Polythylene naphthalate (PEN) and polyester (PS). But, these polymer flexible substrates suffer from the disadvantages that they cannot withstand higher temperatures and the possibility of formation of crack in the seed layer films [34]. Hence, a flexible metal alloy substrate that is thermally and electrically conductive & can easily withstand higher temperatures will be a good alternative for the growth of nanorods as well as for sensor fabrication process [35]. The use of electrically-conductive flexible substrate as one of the electrodes reduces the overall device fabrication process step. During the recent years, our group is one of the fore-front groups in exploring the above mentioned advantage of flexible conductive substrates. In this regard, we have reported our works on the integration of piezoelectric

ZnO thin films on flexible metal alloy substrate for various thin film sensor applications such as impact sensor [36], vibration sensor [37] and flow sensor [38]. However, considering the wide applicability of 1D ZnO nanostructures, it is important to explore high-quality ZnO nanorods synthesis on various metal alloy substrates for the realization of different piezoelectric devices.

In the present paper, we are reporting the detailed studies performed on the synthesis of ZnO nanorods over a novel substrate namely Phynox alloy. In our work, we have adopted low temperature solution growth method for the synthesis of ZnO nanorods. In addition to the general characterization of the as-synthesized ZnO nanorods, their wetting behaviour analysis was also performed to confirm that whether they are hydrophobic or hydrophilic in nature.

2. Experimental

2.1. Selection of Phynox alloy substrate

In the present work, we have chosen Phynox (Elgiloy, Lamineries, MATTHEY SA) as a substrate, which is cobalt chromium based alloy (40% Co, 20% Cr, 16% Ni, 7% Mo, (*Table 1*, Supplementary info.)), flexible and thermally & electrically conductive [39]. Here, Phynox alloy serves both as the substrate for the synthesis of ZnO nanorods and as the bottom electrode in the device fabrication process. Further, it can easily withstand temperatures from−268.8 °C to about 500 °C, extremely resistant to corrosion and also biocompatible. Hence, the selection of the Phynox alloy substrate has several advantages namely; as mentioned before, it reduces the overall complexity of synthesis and device fabrication process in comparison with other non-conducting flexible substrates and also helpful for improving the performance characteristics of the possible resulting devices.

2.2. Synthesis of ZnO nanorods on Phynox alloy substrate

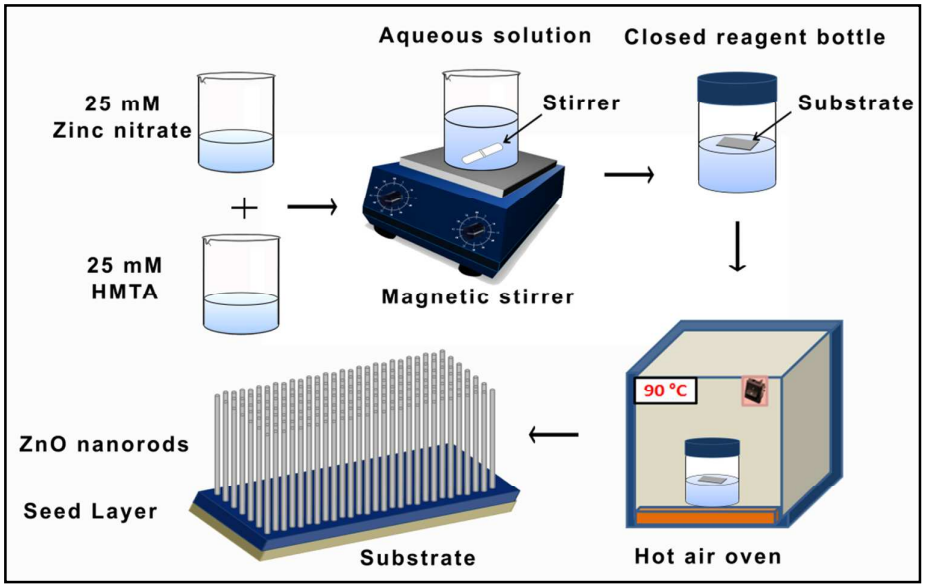

Fig. 1 Block diagram of process steps followed for the synthesis of hydrothermally grown ZnO nanorods.

Different process steps followed for the synthesis of ZnO nanorods are shown in Fig. 1. Prior to synthesis of ZnO nanorods, Phynox alloy substrate was thoroughly cleaned using acetone, isopropyl alcohol and subsequently with DI (de-ionized) water by ultrasonication for 10 minutes. Cleaned alloy substrate was deposited with ZnO seed layer (~100 nm, S1 (a), supplementary info.) by DC reactive-magnetron sputtering. The growth process of nanorods over the seed layer was performed by a simple solution growth assisted hydrothermal method, similar to the method followed in our previous work [9, 13]. In this process, an aqueous solution consisting of an equal amount of zinc nitrate hexahydrate ($Zn(NO_3)_2.6H_2O$) and hexamethylenetetramine (HMTA, $C_6H_{12}N_4$) with the concentration of 25 mM was prepared. The ZnO-film-coated substrate was placed over the surface of solution (~ 60 ml) in a screw reagent bottle. Subsequently, ZnO-coated substrates were maintained at growth temperature of 90 °C for 4 hours

duration by keeping the closed bottle inside the hot air oven. In order to study the temperature influence over morphology of ZnO nanorods, the growth temperature was varied from 50-90 °C separately while maintaining all other process parameters constant. The growth process of ZnO nanorods involves the below mentioned chemical reactions [40].

Decomposition reaction:

$$(CH_2)_6N_4 + 6\,H_2O \longleftrightarrow 4\,NH_3 + 6HCHO$$

Hydroxyl supply reaction:

$$NH_3 + H_2O \longleftrightarrow NH^{4+} + OH^-$$

Supersaturation reaction:

$$Zn^{2+} + 2OH^- \longleftrightarrow Zn\,(OH)_2$$

ZnO nanorod growth reaction:

$$Zn\,(OH)_2 \longleftrightarrow ZnO + H_2O$$

After the growth process, the substrates were allowed to cool down to room temperature. Further, the ZnO -coated substrates were taken out and thoroughly cleaned with DI water for removing the organic salts and these were allowed to dry at room temperature [3, 13, 29, 40]. After this process, the formations of white coloured nano-structured films were observed over the substrates.

2.3. Characterization

As-synthesized ZnO nanostructures on Phynox alloy substrate were characterized by the following techniques.

Bruker D8 Advance diffractometer (Model no: A18-A100/ D76182) was used for X-ray diffraction (XRD) studies. Here, the diffractometer was adjusted in reflective mode powered

at 40 kV and 30 mA at room temperature. The Cu Kα radiation (λ = 1.5406 Å), with nickel filter at a scan rate of 2° min^{-1} in the range of 10-90°, were used to examine the crystalline phase of the films.

Microscopic images were acquired using Field-emission scanning electron microscopy (FE-SEM) (Carl Zeiss, Ultra 55) instrument equipped with SE2 and InLense detectors. Here, the accelerating voltage was maintained between 5-10 kV. Energy dispersive X-ray spectroscopy (EDXS) measurements were carried out with the same instrument equipped with an Oxford INCA x-sight X-ray detector. The EDXS data was acquired at an accelerating voltage of 15 kV.

Transmission electron microscopy (TEM) and high resolution (HR-TEM) analyses were also carried out using a TEM, F30, Tecnai30 D264 S-Twin microscope operated at 300 kV and having a 0.14 nm point resolution. The TEM-sample was prepared specially by scraping the nanorods from the Phynox alloy substrate and dispersed them in acetone solution. The solution dispersed with nanorods was subjected to ultrasonication for 10 min. Finally, the solution was drop casted onto a carbon coated copper grid and dried.

X-ray photoelectron spectroscopy (XPS, Kratos Axis Ultra DLD system) spectrum analysis were performed using Al Kα radiation dual anode source (Energy, hυ = 1486.6 eV) with X-Ray power 150W in ultra high vacuum environment (base pressure of 3 x 10^{-9} Torr). All XPS peaks were calibrated with respect to carbon (C 1s) at 284.8 eV. The XPS spectra were recorded at constant pass energy of 160 eV for survey scans and 20 eV for high-resolution scans. The data fitting and quantification analysis were carried out using CASA XPS software after considering the relative sensitivity factors (RSF) for each element of the compound. Gaussian–Lorenzian functions and Shirley type background were employed during the analysis.

2.4. Wetting behaviour analysis

The wetting behaviour (hydrophobic/hydrophilic) analysis was studied by water contact-angle (WCA) measurements. The WCA measurements were performed over the as-synthesized ZnO nanorods on Phynox alloy substrate using optical contact angle measuring instrument (Data Physics, Model # OCA 30/6), using the sessile drop method. A 2-µl droplet of DI water was positioned on the surface via a micro syringe and images were captured to measure the contact-angle formed at the interface of liquid to the solid surface. The contact angle was calculated via fitting experimental data by the software (SCA 20).

3. Results and Discussion

The surface morphologies of as-grown ZnO nanostructures on flexible Phynox alloy substrate at different growth temperatures in the range of 60 to 90 °C are shown in Fig. 2 (a)-(d) respectively. As can be seen in the FE-SEM images, the ZnO nanorods are present all over the substrate and are uniformly distributed. The cross-sectional view of the ZnO nanorods is shown in the inset Fig. 2 (a)-(d). As can be observed by the FE-SEM images and measured average tilt angles (*Table 2*, supplementary info.) of nanorods with respect to the substrate confirms that the orientations of the ZnO nanorods are in relatively vertical to the substrate. *Table 3* (supplementary info.) shows the average length and diameter of the as-grown ZnO nanorods for the growth temperature of 60, 70, 80 and 90 °C, respectively. It can be observed that, the length and diameter of the ZnO nanorods, increased with the increase of growth temperature (Fig. 3 (a)-(b)). Hence, it is clearly evident that the growth temperature has a pronounced effect on the morphology in terms of length as well as diameter of nanorods. It means that the aspect ratio of the nanorods also increases with the raise of growth temperature (Fig. 3 (c)). Similar study has been reported by Willander *et al.*, wherein the effect of growth temperature on the aspect ratio and morphology of nanorods on the Si

substrate has been studied [41]. Also Wang et al., have attempted a similar kind of studies (growth temperature effect on the aspect ratio of ZnO nanorods) on Au coated Si substrate on basis of crystal nucleation and growth theory. It was found that the diffusion length and mobility of ions is critically depends upon the growth temperature [42]. Considering the same theory for the present work, at higher temperature (90 °C), the mobility and diffusion length of the ions (Zn^{+2} and OH^{-}) are large enough in the precursor solution to reach the sites of the nuclei for the subsequent growth of nanorods. Thus, these precursor ions exhibit higher affinity towards the already-formed seeds. Moreover, at 90 °C, HMTA decomposes promptly in order to provide sufficient number of hydroxide ions (OH^{-}) resulting in higher vertical growth rate. The above discussed phenomenon is considered to be the main reason behind higher aspect ratio (i.e., 12.265) of nanorods grown at 90 °C. In similar way, at the lower temperature (60 °C), due to the lower decomposition rate of HMTA the mobility and the diffusion length of the Zn^{+2} and OH^{-} ions on the substrate are rather limited, which prohibit the ions diffusion, and consequently lower aspect ratio (i.e., 1.97). Considering it being an aqueous solution based hydrothermal method, the growth temperature studies has been performed below 100 °C [41]. Further, in order to observe the lower limit of the growth temperature, the nanorods growth study was performed at temperature 50 °C. Interestingly, the nanorods growth was not noticed on the substrate at the growth temperature of 50 °C. This can be due to insufficient thermal energy at 50 °C, the incomplete decomposition of HMTA ultimately affecting the concentration of hydroxide ions which affects improper ZnO nucleation as well as nanorods growth. Therefore, it is concluded that the nanorods growth starts above the temperature of 50 °C (S2 (a-b), supplementary info.).

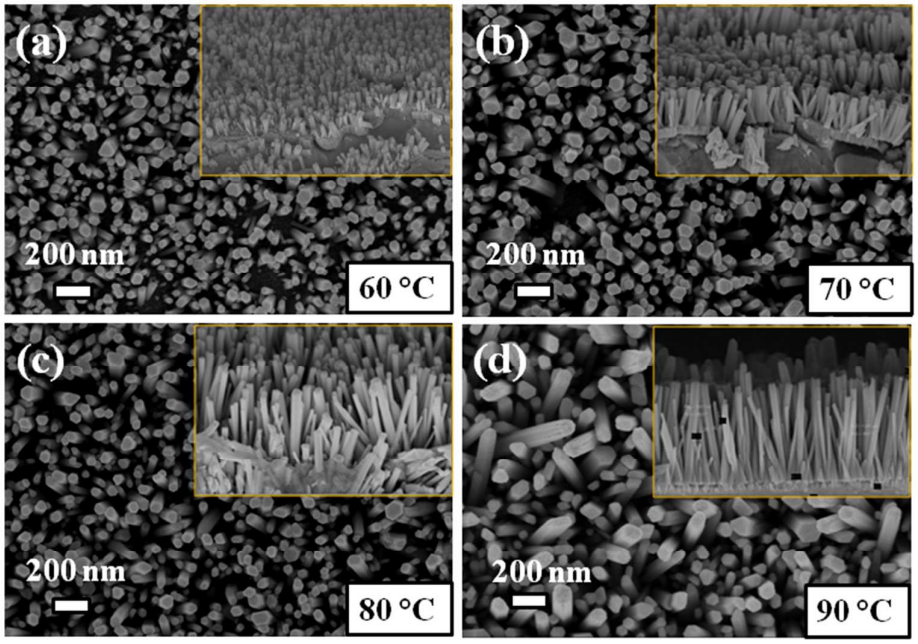

Fig. 2 FE-SEM images for the as-grown ZnO nanorods at different growth temperatures of (a) 60 °C, (b) 70 °C, (c) 80 °C, (d) 90 °C. (Note: inset figures show the corresponding cross-sectional images).

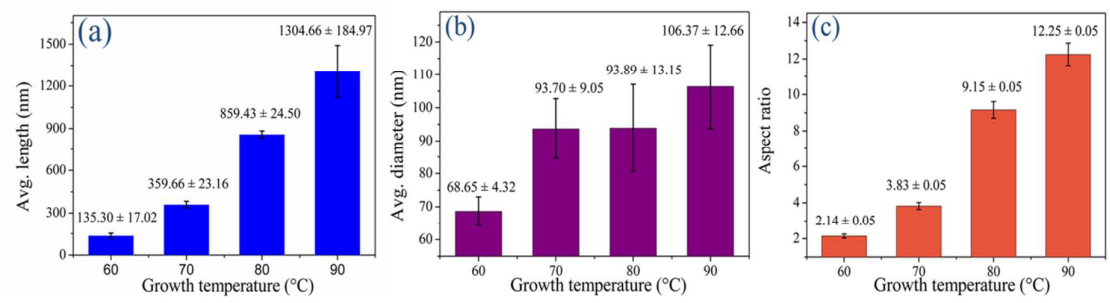

Fig. 3 (a) Growth temperature vs avg. length (b) Growth temperature vs avg. diameter (c) Growth temperature vs aspect ratio of ZnO nanorods.

Further, energy dispersive X-ray spectroscopy (EDXS) analysis was also performed on the surface of the ZnO nanorods grown at 90 °C (Fig. 4 (a)-(b)), primarily to confirm the presence of Zn and O atoms and also to confirm any foreign impurities are present. The presence of Cr and Co elements is because of the substrate Phynox, which is basically an

alloy, composed of Cr-Co. It may be noted that Au (~ 10 nm) was sputtered on the synthesized ZnO nanorod films in order to avoid the charging during SEM imaging (Fig. 4 (b).

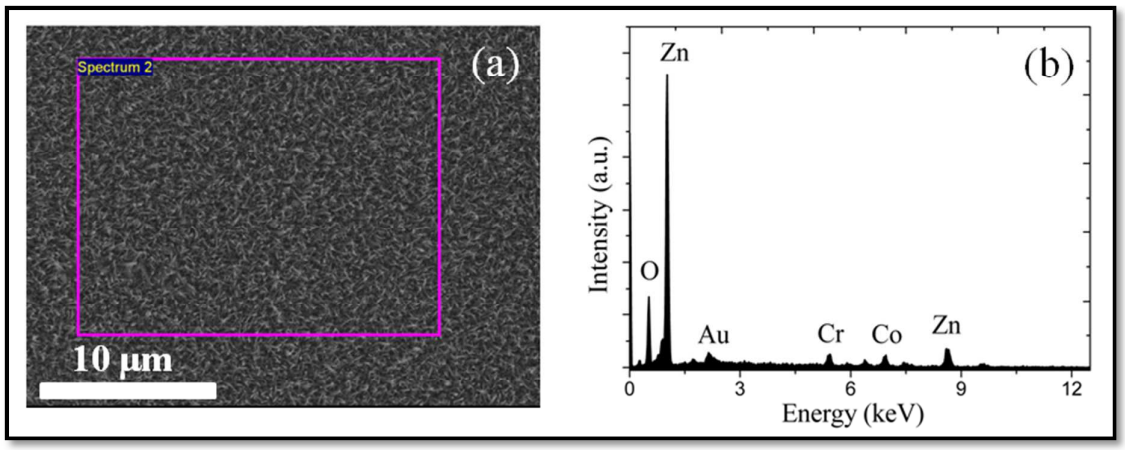

Fig. 4 (a) Lower magnification FE-SEM image of as-grwon ZnO nanorods (90 °C of growth temperature), (b) The EDXS spectrum corresponds to the scanned area.

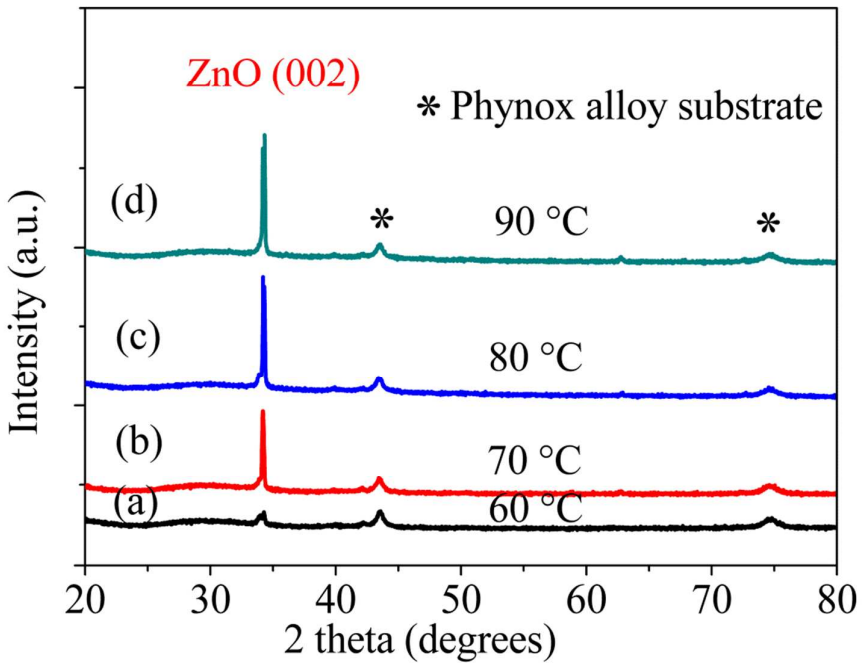

Fig. 5 XRD pattern for the ZnO nanorods on Phynox alloy substrate at different growth temperatures of (a) 60 °C, (b) 70 °C, (c) 80 °C,(d) 90 °C.

The X-Ray diffraction pattern recorded on the ZnO nanorods grown at different growth temperatures (60-90 °C) are shown in Fig. 5 (a)-(d). The highest intensity diffraction peak at 2θ=34.3° is the corresponding plane (002) of ZnO nanorods and it was observed with the growth temperature of 90 °C in Fig. 5(d). (JCPDS # 36-1451). In all the cases, a high intense diffraction peak was observed at 34.3° (002), which indicates that the ZnO nanorods are strongly oriented along (002) [29,40,41]. Furthermore, the sharp and narrow diffraction peaks indicate that the ZnO nanorods have good crystallinity. The full width at half maxima (FWHM) and d-spacing values of as-grown ZnO nanorods (grown at 90 °C) were found to be 0.126° and 0.261 nm, respectively. The other peaks appeared at 2θ value of 43.5° and 74.6° are the major substrate (bare Phynox alloy) elements (S4, supplementary info.). These substrate peaks are marked with "*" as Phynox alloy substrate. Moreover, the observed nanorods grown at 60 °C growth temperature (Fig. 5 (a)) showed poor crystalline nature compared to those grown at 90 °C. It is observed that the high intense peak at 34.3° (002) is gradually increased when the growth temperature is increased from 60 to 90 °C. Yet, all the samples showed similar kind of XRD patterns except in the intensity variations. The FWHM values for the ZnO nanorods grown at different growth temperatures (60-90 °C) are also relatively reduced as the growth temperature increased (S4, supplementary info.). Likewise, the XRD pattern was recorded for the growth temperature of 50 °C (S2 (c), supplementary info.). Considering the negligible nanorods growth at 50 °C, the observed intensity peak at 2θ=34.3° is believed to be due to the ZnO seed layer film.

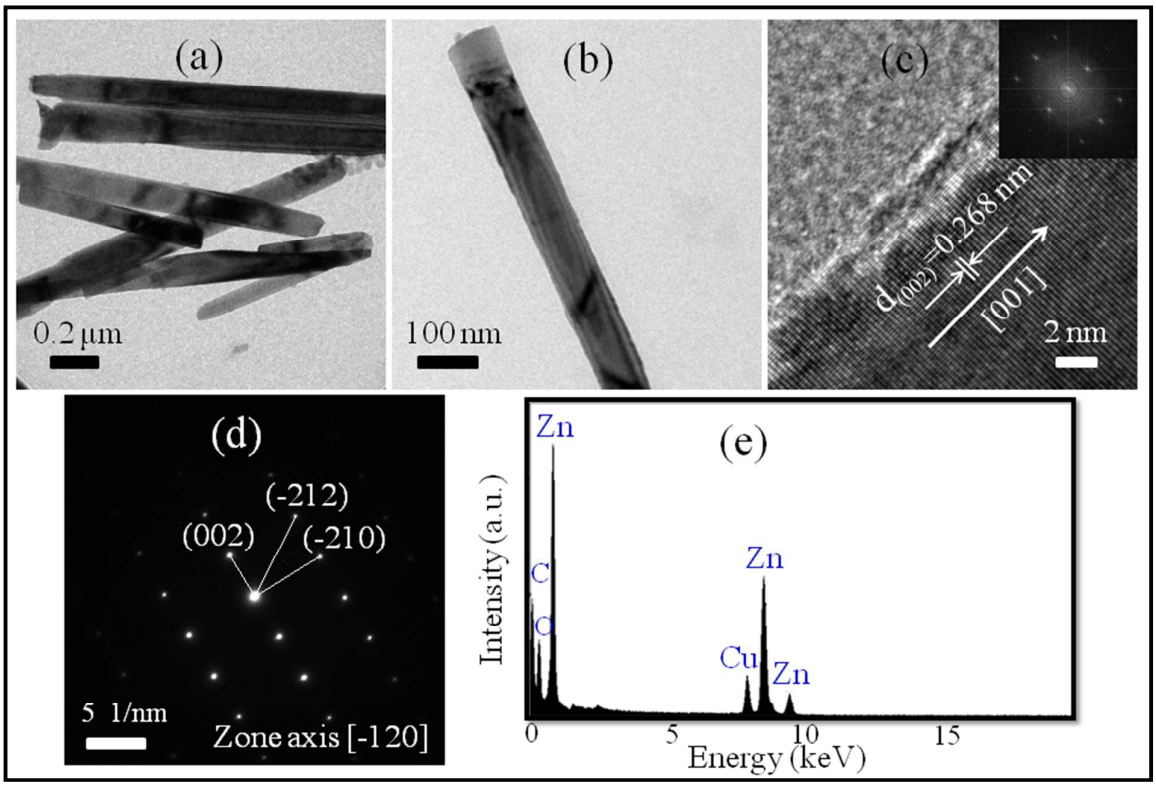

Fig. 6 TEM analysis of ZnO nanorods with 90 °C growth temperature, (a) Low magnification image, (b) Higher magnification of single nanorod, (c) HR-TEM image (inset shows the corresponding FFT image), (d) SAED pattern, and (e) Corresponding EDS pattern.

Apart from the above, structural characterization and composition analysis of single ZnO nanorod was also carried out using TEM. Low and high magnification bright field images of nanorods are shown in Fig. 6(a) and (b) respectively. These nanorods confirm the 1D nature of the ZnO nanorod. The captured single nanorod diameter is about 95 nm (Fig. 6 (b)). The dimensions of the nanorods under TEM observation are in good agreement with the FE-SEM results. The HR-TEM (High Resolution-TEM) image of single ZnO nanorod is shown in Fig. 6(c) and it indicates that the growth direction is along with (001) facet [43, 44]. The measured d-spacing value from HR-TEM image and its FFT image (local diffraction, inset Fig. 6(c)) is found to be 0.268 nm, which corresponds to inter-planar spacing of (002) plane in ZnO [45]. There were no noticeable crystalline defects in the ZnO nanorod found in

the HR-TEM image, which indicates a good quality crystalline structure. Fig. 6(d) shows the selected area electron diffraction (SAED) pattern recorded on the same ZnO nanorod and it was taken under [-120] zone axis. Sharp and clear diffraction spots were observed, which indicate the fact that the ZnO nanorods have a good single-crystalline structure grown along *c*-axis direction. The reflections correspond to (002), (-210) and (-212) lattice planes of ZnO with hexagonal structure indexed [44, 45]. The EDXS measurement recorded on the single ZnO nanorod is shown in Fig. 6(e) wherein the presence of Zn, O, Cu and C elements are clearly evident. The presence of Cu and C elements are due to the carbon-coated TEM grid used for TEM analysis.

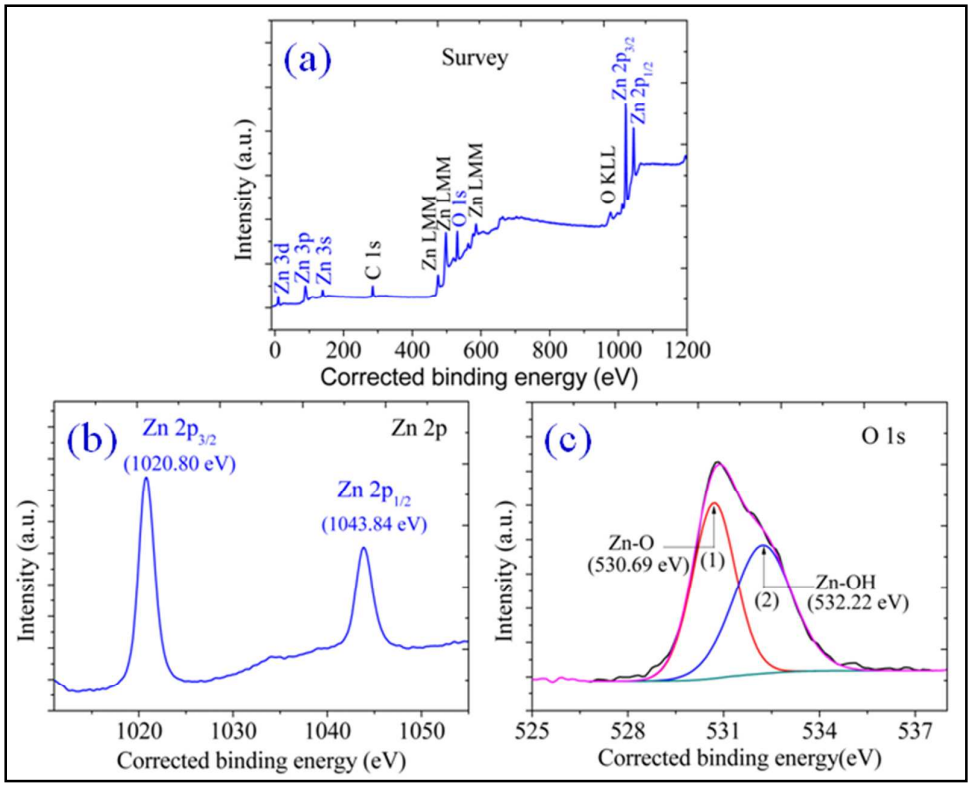

Fig. 7 (a) XPS survey spectra, (b) Zn 2p peak and (c) O 1s peak.

Further, surface analysis, chemical composition and oxidation state of as-grown ZnO nanorods were measured by XPS. Zn, O and C peaks were detected as shown in the survey spectra in Fig. 7 (a), indicating that no elements were found other than C. The detected C is

related to the carbon adsorbed on the surface during the exposure of the sample to the ambient atmosphere. All peaks were calibrated with respect to carbon (C 1s) at 284.8 eV [46, 13]. Fig. 7 (b) shows the high resolution XPS spectra of the Zn 2p region. The Zn 2p core-level of ZnO nanorods has two fitting peaks located at about 1020.80 eV and 1043.84 eV attributed to Zn $2p_{3/2}$ and Zn $2p_{1/2}$, respectively. These results indicate that the chemical valence (oxidation state) of Zn at the surface morphology of ZnO is +2. The binding energy difference between the $Zn2p_{1/2}$ and $Zn2p_{3/2}$ is 23 eV for morphology of ZnO. These values are in good agreement with the reported ZnO nanorods [46-47]. In addition to that, the measured Auger parameter of Zn value (2009.61 eV) is in close agreement with the previously reported ZnO nanostructures, which confirms the formation of ZnO [48, 13]. Fig. 7 (c) displays the XPS spectra of O 1s region of ZnO nanorods. It is demonstrated that the O 1s core-level spectrum of ZnO nanorods involves two different forms of oxygen. Two fitting Gaussians peaks marked as (1) and (2) were used to fit the experimental data. Peak (1), positioned at the lower binding energy of 530.69 eV, and is assigned to O^{2-} ions in the Zn–O bonding of the wurtzite structure of ZnO. The other peak (2) located at 532.2 eV is related to OH^- group absorbed onto the surface of the ZnO nanorods. These values are in good agreement with the reported work of ZnO nanorods [46- 47].The detailed quantification data of ZnO nanorods is provided in the supplementary information (*Table 4*). In this, the binding energy (BE) for the core levels of Zn 2p & O 1s, corresponding FWHM values and their respective atomic concentrations are listed.

4. Application: Contact angle measurements for surface analysis of the ZnO nanorods

The surface wettability (hydrophobicity or hydrophilicity) nature of the synthesized ZnO nanorods is determined by knowing the water contact angle (WCA) measurements. If the solid surface of nanorods has a contact angle with liquid droplet (DI water) that is greater than 90 °, then the surface is classed as hydrophobic and if the contact angle is less than 90 °,

the surface is hydrophilic in nature [49-50]. Fig. 8 (a)-(d) shows the variation of the WCA measurements with growth temperature (60-90 °C) for the as-grown ZnO nanorods. The ZnO nanorods with different growth temperatures show the WCA of 117.90° ± 2.42°, 137.96 ° ± 1.79°, 137.00° ± 1.95° and 139.53° ± 2.36° respectively (*Table 5*, supplementary info.). All the measurements were carried out at the same conditions. As can be seen in the images (Fig. 8 (a)-(d)), for all the samples the observed WCA is greater than the 90°.Therefore, we can conclude that the synthesized ZnO nanorods are hydrophobic in nature. The measured WCA of the nanorods grown even at 50 °C is 103.56° ± 1.92°, which is mainly from the ZnO seed layer and not from the nanorods (S2 (d), supplementary info.). The increase of growth temperature resulted in different WCA of the ZnO nanorods (Fig. 9). *Hsieh.et al.*, reported that the variation of the WCA is mainly because of height variation of ZnO nanorods, which indirectly reveals the fact that the aspect ratio of ZnO nanorods plays an important role for the variation of WCA. Therefore, it is possible that the morphology of ZnO nanorods and their aspect ratio are responsible in preventing the penetration of water droplet due to a large amount of air trapped in the interspaces between each nanorod in nano scale level [51]. *Wang. et al*., reported the variation of WCA with respect to aspect ratio, growth time and growth temperature [52]. In the work reported by *Gong.et al.,* the variations of WCA are based on the changes in surface roughness of the nanowires [53]. From above references, it can be deduced that morphology and surface roughness variation affect WCA. In the present work, the observed change in aspect ratio (i.e. variation of height/diameter ratio) due to dissimilar rate of increase in height and diameter (Table 2, supplementary info.). There is a significant change in WCA from 50 to 70 °C due to aspect ratio as well as increased air trappings which tends to saturated at higher temperature (≥ 70 °C) due to higher influence of surface roughness of nanorods forest. The WCAs are closely identical only above 70 °C samples. It is believed that the minor variations of the WCAs are due to the small variations

of surface roughness of the nanorods. The change in the surface roughness can be clearly seen in the top view of SEM images (Fig 2). For samples grown at ≤ 70 °C, the factor playing important role in determining the WCA is the air trapped between these nanorods which will be decided primarily by height of nanorods (the Cassie–Baxter model) and up to certain extent also by aspect ratio. This is because the aspect ratio will also affect by the surface roughness of nanorods-forest along with the air trapped between them. The change in the surface roughness can change the WCA irrespective of their aspect ratio/ height of the nanorods. Finally, we conclude that the WCA variations with the raise of growth temperature not only depend upon height/aspect ratio but also depend on morphology (surface roughness) of ZnO nanorods.

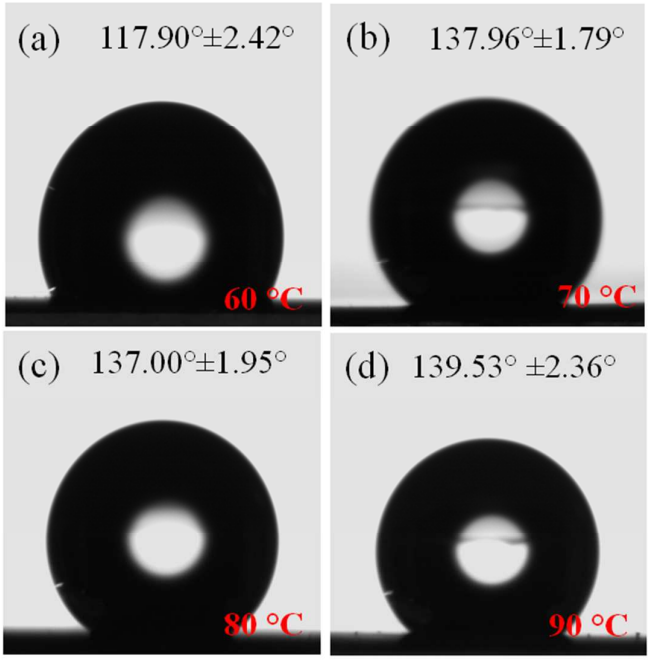

Fig. 8 Water contact angle (WCA) measurements over the surface of ZnO nanorods for the growth temperature of (a) 60 °C, (b) 70 °C, (c) 80 °C, (d) 90 °C.

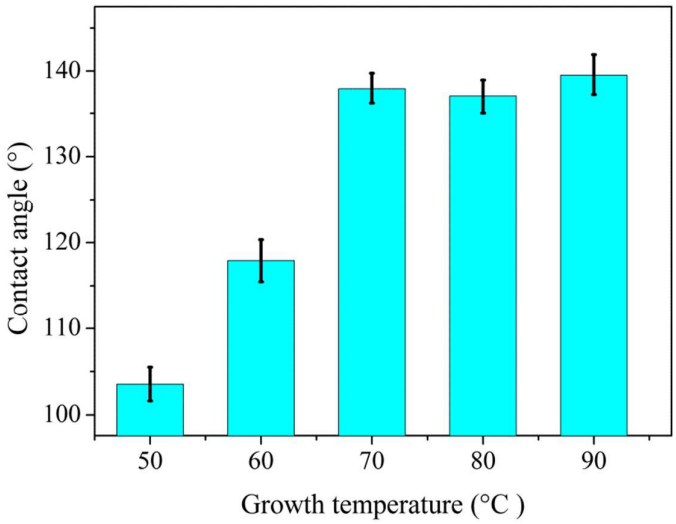

Fig.9 WCA measurements with respect to growth temperatures.

5. Conclusions

Highly-oriented ZnO nanorods are successfully synthesized on a novel flexible Phynox alloy substrate by altering the growth temperature parameter in the low-temperature solution growth method. The growth temperature was varied from 50-90 °C in steps of 10 °C. This novel Phynox substrate which is electrically conductive, can easily withstand wide temperature range (-268.8 to 500 °C), extremely resistant to corrosion and also biocompatible paves way for not only eases the fabrication by avoiding one of the electrode deposition step but also improves the reliability as well as self-life of the fabricated device. Considering these advantages, Phynox may be useful for a verity of material synthesis processes as well as flexible electronics. Due to its biocompatibility, the alloy substrate can be used in biomedical applications especially in peacemakers (implantable medical device) as one of the electrode. Phynox material in different forms is used as springs, seal components and components for watches. Furthermore, several industries such as aerospace, telecommunication, petrochemical, marine engineering and process control plants also employ Phynox alloy strips are used as membranes for pressure sensors and some cases in relays and switches. The

study of temperature dependant synthesis of ZnO nanorods is brought an insight in term of variations in their aspect ratio and subsequently brought an idea of their wettability property (hydrophobicity). Integration of as-synthesized ZnO nanorods grown on flexible Phynox alloy substrate can offer various device application possibilities namely self cleaning devices, sensors (impact, flow, pressure and acoustic) & micro-actuators and energy harvesting devices likes nanogenerators.

Acknowledgments

The authors are grateful to SERB, DST, Govt. of India for kindly supporting the work reported in this paper, in the form of project (Project No# SB/EMEQ-320/2013). The authors are also thankful to the Advanced Facility for Microscopy and Microanalysis (AFMM), IISc, for providing the microscopy facility. Authors also wish to thank the Centre for Nano Science and Engineering (CeNSE) for providing the FE-SEM and XPS facility, IISc. Thanks to the IPC department for providing XRD facility, IISc. The authors gratefully acknowledge Prof. Satish Vasu Kailas (Dept. of Mechanical Engg), IISc, for allowing us to use the water contact angle measurement facility.

References

[1]. Z. L. Wang, *J. Phys.: Condens. Matter*, 2004, 6 (25), R829–R858.
[2]. B. Kumar and S. W. Kim, *Nano energy*, 2012, 1(3), 342-355.
[3]. S. Xu and Z. L. Wang, *Nano Research*, 2011, 4 (11), 1013-1098.
[4]. Z. L. Wang, *Applied Physics A*, 2007, 88(1), 7-15.
[5]. C. S. Lao, P. X. Gao, R. S. Yang, Y. Zhang,Y. Dai and Z. L. Wang, *Chemical Physics Letters*, 2006, 417(4), 358-362.
[6]. F. Li, Y. Ding, P. Gao, X. Xin, and Z. L. Wang, *Angew. Chem. Int. Ed.*, 2004, 43(39), 5238–5242.
[7]. R. Yang, Y. Ding and Z. L. Wang, *Nano Letters*, 2004, 4(7), 1309-1312.

[8]. Z. W. Pan, Z. R. Dai and Z. L. Wang, *Science*, 2001, 291(5510), 1947-1949.

[9]. V. Gaddam, S. Joshi, M. Parmar, M. M. Nayak and K.Rajanna, *IEEE Sensors*, 2012, 1870-1873.

[10]. P. X. Gao, Y. Ding and Z. L. Wang, *Nano Letters*, 2003, 3(9), 1315-1320.

[11]. G. W. She, X. H. Zhang, W. S. Shi, X. Fan, J. C. Chang, C. S. Lee, S.T. Lee and C.H. Liu, *Applied physics letters*, 2008, 92(5), 3111.

[12]. X. L.Yu, H. M. Ji, H. L. Wang, J. Sun and X. W. Du, *Nanoscale research letters*, 2010, 5(3), 644-648.

[13]. V. Gaddam, R. R. Kumar, M. Parmar, G. R. K. Yaddanapudi, M. M. Nayak and K.Rajanna, *RSC Adv.*, 2015, 5, 13519.

[14]. M. H. Huang, S. Mao, H. Feick, H. Yan , Y. Wu, H. Kind, E. Weber, R. Russo, and P. Yang, Science, 2001, 292(5523), 1897-1899.

[15]. K. Govender, D.S. Boyle, P. O'Brien, D. Binks, D. West and D. Coleman, Advanced Materials, 2002, 14(17), 1221-1224.

[16]. W. I. Park and G.C. Yi, *Advanced Materials*, 2004, 16(1), 87-90.

[17]. Y. W. Zhu, H.Z. Zhang, X.C. Sun, S.Q. Feng, J. Xu, Q. Zhao, R.M. Wang and D.P. Yu, *Applied Physics Letters*, 2003, 83(1), 144-146.

[18]. W.Z. Wang, B.Q. Zeng, J. Yang, B. Poudel, J. Y. Huang, M.J. Naughton and Z.F. Ren, *Advanced Materials*, 2006, 18(24), 3275-3278.

[19]. M. Law, L.E. Greene, J.C. Johnson, R. Saykally and P.Yang, *Nature materials*, 2005, 4(6), 455-459.

[20]. Y. Wei, C. Xu, S. Xu, C. Li, W. Wu and Z. L. Wang, *Nano letters*, 2010, 10(6), 2092-2096.

[21]. C. R. Gorla, N. W. Emanetoglu, S. Liang, W.E. Mayo, Y. Lu, M. Wraback and H. Shen, *Journal of Applied Physics*, 1999, 85(5), 2595-2602.

[22]. X. Wang, J. Zhou, J. Song, J. Liu, N. Xu and Z. L. Wang, *Nano letters*, 2006, 6(12), 2768-2772.

[23]. B. A. Buchine, W. L. Hughes, F.L. Degertekin and Z. L. Wang, *Nano letters*, 2006, 6(6), 1155-1159.

[24]. S. Xu, Y. Qin, C. Xu, Y. Wei, R. Yang and Z. L. Wang, *Nature nanotechnology*, 2010, 5(5), 366-373.

[25]. J. J. Wu and S. C. Liu, *Advanced Materials*, 2002, 14(3), 215.

[26]. W. I. Park, D. H. Kim, S. W. Jung and G. C. Yi, *Applied Physics Letters*, 2002, 80(22), 4232-4234.

[27]. Y. W. Heo, V. Varadarajan, M. Kaufman, K. Kim, D. P. Norton, F. Ren and P. H. Fleming, *Applied physics letters*, 2002, 81(16), 3046-3048.

[28]. Y. Sun, G. M. Fuge and M. N. Ashfold, *Chemical Physics Letters*, 2004, 396(1), 21-26.

[29]. L. Vayssieres, *Advanced Materials*, 2003, 15(5), 464-466.

[30]. Z. Yin, S. Wu, X. Zhou, X. Huang, Q. Zhang, F. Boey and H. Zhang, *Small*, 2010, 6(2), 307-312.

[31]. J. Nayak, S.N. Sahu, J. Kasuya and S. Nozaki, *Journal of Physics D: Applied Physics*, 2008, 41(11), 115303.

[32]. J. Liu, X. Huang, Y. Li, X. Ji, Z. Li, X. He and F. Sun, *The Journal of Physical Chemistry C*, 2007, 111(13), 4990-4997.

[33]. T. Ngo-Duc, K. Singh, M. Meyyappan and M. M. Oye, *Nanotechnology*, 2012, 23(19), 194015.

[34]. C. L. Hsu and K.C. Chen, *The Journal of Physical Chemistry C*, 2012, 116(16), 9351-9355.

[35]. S. Joshi, M. M. Nayak and K. Rajanna, *Proc. IEEE Sens.*, 2012, 1866-1869.

[36]. S. Joshi, G. M. Hegde, M. M. Nayak and K. Rajanna, *Sensors and Actuators A: Physical*, 2013, 199, 272-282.

[37]. S. Joshi, M. M. Nayak and K. Rajanna, *Applied Surface Science*, 2014, 296, 169‑176.

[38]. S. Joshi, M. Parmar and K. Rajanna, *Sensors and Actuators A*, 2012, 187, 194‑200.

[39].http://www.matthey.ch/fileadmin/user_upload/downloads/fichetechnique/EN/Phynox_C.pdf.

[40]. Y. Zhang, M. K. Ram, E. K. Stefanakos, and D. Y. Goswami, *Journal of Nanomaterials,* 2012, 2012, 1-22.

[41]. G. Amin, M. H. Asif, A. Zainelabdin, S. Zaman, O. Nur, andM.Willander, *Journal of Nanomaterials*, 2011, 2011, 1-8.

[42]. S. Xu, C. Lao, B. Weintraub and Z. L. Wang, *J. Mater. Res.,* 2008, 23(8), 2072-2077.

[43]. H. Li, C. Liang, K. Zhong, M. Liu, G. A. Hope, Y. Tong and P. Liu, *Nanoscale Res Lett,* 2009, 4 (10), 1183–1190.

[44]. H. K. Park, S. P. Hong and Y. R. Do, *Journal of the Electrochemical Society*, 2012, 159 (6), D355-D361.

[45]. F. Ahmed, S. Kumar, N. Arshi, M. S. Anwar and B. H. Koo, *CrystEngComm*, 2012, 14, 4016–4026.

[46]. R. Al-Gaashani, S.Radiman, A.R.Daud, N.Tabet and Y.Al-Douri, *Ceramics* International, 2013, 39(3), 2283-2292.

[47]. V. P. Dinesh, P. Biji, Anuradha Ashok, S. K. Dhara, M. Kamruddin, A. K. Tyagi and Baldev Raj, *RSC Adv*., 2014, 4, 58930.

[48]. S. Bera, S. Dhara, S. Velmurugan, and A. K. Tyagi, *International Journal of Spectroscopy*, 2011, 2012, 1-4.

[49]. J. Lv, J. Zhub, K. Huangd, F. Menga, X. Songa and Z. Sun, *Applied Surface Science*, 2011, 257 (17), 7534–7538.

[50]. P. R. Elliott, S. P. Stagon, H. Huang, D. U. Furrer, S. F. Burlatsky and T. P. Filburn, *Scientific reports,* 2015, 5:9260.

[51]. C. T. Hsieh, S. Y. Yang and J. Y. Lin, *Thin Solid Films*, 2010, 518 (17), 4884–4889.

[52]. G. He and K. Wang, *Applied Surface Science*, 2011, 257 (15), 6590–6594.

[53]. M.G. Gong, Y.Z. Long, X.L. Xu, H.D. Zhang and B. Sun, "Synthesis, Superhydrophobicity, Enhanced Photoluminescence and Gas Sensing Properties of ZnO Nanowires", *TECH Open Access Publisher*, 2012, ch.5, 77-100.